

Contents lists available at ScienceDirect

# Journal of Electroanalytical Chemistry

journal homepage: www.elsevier.com/locate/jelechem



# Molybdenum diselenide formation using electrochemical atomic layer deposition (E-ALD)



Chu F. Tsang, Maria A. Ledina, John L. Stickney\*

Department of Chemistry, University of Georgia, Athens, GA 30602, United States

# ARTICLE INFO

Article history:
Received 21 November 2016
Received in revised form 25 January 2017
Accepted 31 January 2017
Available online 3 February 2017

Keywords:
Electrochemical Atomic Layer Deposition (E-ALD)
Molybdenum diselenide thin films
Underpotential deposition
Molybdenum electrodeposition
Selenium electrodeposition
Cyclic voltammetry

# ABSTRACT

Cyclic voltammetry (CV) of Au in  $MoO_3$  and  $SeO_2$  solutions was studied under both basic and acidic conditions, as a precursor to development of E-ALD cycle chemistry for the electrodeposition of  $MoSe_2$ . Those results indicated that acidic  $HMoO_4^-$  and  $SeO_2$  precursor solutions would be a better choice for the formation of  $MoSe_2$  using E-ALD. Photoelectrochemical (PEC) photovoltage measurements revealed an optical band gap of 1.1 eV for the as-deposited  $MoSe_2$  films. Some unreacted  $MoO_2$  was detected by the PEC measurements, as well, but were removed by thermal annealing. Some excess elemental Se was also removed during the anneal, and Raman spectroscopy indicated that the films' crystallinity was improved. Deposit quality was followed using X-ray photoelectron spectroscopy (XPS), Raman spectroscopy, and electron probe microanalysis (EPMA). Se appeared to suppress Mo oxidation and induce  $MoSe_2$  film growth in the E-ALD cycle.

© 2017 Elsevier B.V. All rights reserved.

### 1. Introduction

Graphene is the epitome of a 2-dimensional (2D) material and has garnered great attention recently [1]. Another category of 2D materials is the transition metal dichalcogenides (TMDC), which are becoming increasingly important to material chemists, physicists, and engineers. TMDCs have the general formula  $MX_2$ , where M is a transition metal (such as Ta, Nb, Mo, or W) and X is a chalcogen (S, Se, or Te) [2]. Each layer of  $MX_2$  is a trilayer, made up of a sandwich of two chalcogen layers on either side of a transition metal center layer. The trilayers are held together via van der Waals interactions in the bulk material, and different structural polytypes exist depending on the stacking sequence [3].

TMDCs exhibit numerous intriguing properties, suggesting a wide range of potential applications. One such property is the ability of some TMDC to undergo Peierls transitions to form charge density waves (CDW) [4]. The possibility of utilizing CDW in electronic device applications has been considered, stimulating a desire to try and grow TMDC nanofilms layer-by-layer with an alternative growth method [5,6]. Preliminary electrodeposition studies of chalcogens

onto Ta substrates by this group yielded promising results, affirming electrodeposition as a viable option for growing TMDC [7].

In the study presented here, Electrochemical Atomic Layer Deposition (E-ALD) was used to grow molybdenum diselenide (MoSe<sub>2</sub>). Whereas conventional ALD is based on the use of gas-phase surface limited reactions, E-ALD is based on the use of electrochemical surface-limited reactions to deposit thin films. Electrochemical surface-limited reactions are generally referred to as underpotential deposition (UPD) [8–14]. In E-ALD, atomic layers of the desired elements are alternately deposited on each other, in a cycle, with the number of cycles performed dictating deposit thickness.

Properties of molybdenum dichalcogenides have been widely investigated for their potential applications. As the material thickness decreases, band gaps of MoS<sub>2</sub> and MoSe<sub>2</sub> exhibit a crossover from indirect to direct transitions in the limit of a single layer [15–17]. Owing to their band gap energies in the UV-visible region, MoS<sub>2</sub> and MoSe<sub>2</sub> have potential uses in photonics and optoelectronics [18,19]. In the area of renewable solar energy research, MoSe<sub>2</sub> has been used as a catalyst for the hydrogen evolution reaction (HER) [20,21]. Group 6 transition metal dichalcogenides, such as MoSe<sub>2</sub> and MoS<sub>2</sub>, are well-suited as photoelectrodes in regenerative electrochemical solar cells because they are less susceptible to photodecomposition. Their photogenerated excitons originate from the non-bonding *d*-orbitals, thus the photo-initiated reactions arising from these transitions do not directly result in bond breaking [22].

<sup>\*</sup> Corresponding author. E-mail addresses: cftsang@caltech.edu (C.F. Tsang), ledina@uga.edu (M.A. Ledina), stickney@uga.edu (J.L. Stickney).

The difficulty in electrodepositing  $MoSe_2$  stems from the negative standard potential for molybdenum, indicating that the HER should thermodynamically occur as well. In theory, Mo electrodeposition can proceed by the following reaction [23,24]

$$MoO_4^{2-} + 4 H_2O + 6 e^- = Mo + 8 OH^-$$
 (1)

 $E^0$  for the reaction is -0.913 V vs. SHE. Mo electrodeposition from an aqueous solution typically exhibits only  $\sim 1\%$  current efficiency, at best, due to the concurrent HER, the dominant side reaction [25,26]. Metallic Mo is more easily electrodeposited as an alloy with Fe, Co, or Ni [27,28]. If Mo is more successfully co-deposited, it might be that Se could help induce Mo electrodeposition [29–32]. The work presented here examines the electrodeposition of Mo in the presence of Se to form MoSe<sub>2</sub>.

#### 2. Experimental

All potentials are reported vs. an Ag/AgCl (3 M KCl) reference electrode (Bioanalytical Systems, Inc.). The Au substrates (EMF Corp) were 100 nm of Au (99.9%) evaporated onto glass slides coated with 5 nm of Ti as an adhesion layer. All solutions were prepared with 18 M $\Omega$  H<sub>2</sub>O from a Milli-O purification system. The MoO<sub>3</sub> solutions were prepared by sonicating, to dissolve the MoO<sub>3</sub> (I.T. Baker, 99.5%) powder, with one NaOH pellet (Fisher Scientific, 99.6%) in ~20 mL H<sub>2</sub>O. The solution was then diluted to its final volume, and the pH was adjusted. The basic MoO<sub>3</sub> solution (pH 8.3) was prepared by addition of NH<sub>4</sub>Cl (Macron Fine Chemicals, ACS grade) prior to dilution. The acidic HMoO<sub>4</sub><sup>-</sup> solution (pH 1.5) was prepared by addition of HClO<sub>4</sub> (J.T. Baker, 60-62%) to the dissolved MoO<sub>3</sub>; no NH<sub>4</sub>Cl was added. The SeO<sub>2</sub> (Alfa Aesar, 99.999%) solutions were prepared by dissolution in H<sub>2</sub>O, and adjustment of the pH with HClO<sub>4</sub> or NaOH. All solutions contained 0.1 M NaClO<sub>4</sub> as a supporting electrolyte. The NaClO<sub>4</sub> stock solution was prepared by neutralizing HClO<sub>4</sub> with NaOH. MoSe<sub>2</sub> powder (99.9%), purchased from Alfa Aesar, was used as a reference for Raman studies.

All electrochemical experiments were performed using an automated flow cell deposition system (Electrochemical ALD, L.C., Athens, GA). The system was composed of solution bottles, connected through Teflon tubes to a solenoid activated Teflon distribution valve. The valve was connected to the electrochemical flow cell, from which solutions flowed through a peristaltic pump to waste. The cell was operated in the 3-electrode mode, with the Au on glass slides. noted above, used as the working electrodes, the 3 M Ag/AgCl reference electrode, and an Au wire inlaid into the cell wall, across from and parallel to the planar working electrode, used as the auxiliary electrode. The cell volume was about 0.3 mL, and the exposed electrode area was 0.7 cm<sup>2</sup>. The whole system was interfaced to a computer to allow remote control of the potentiostat, cell potential, solutions, and flow time. The LabVIEW-based system control software was written in-house. During MoSe<sub>2</sub> deposition, the flow rate was maintained at 15 mL min<sup>-1</sup> for all flow steps in the cycle. CVs were performed at 10 mV s<sup>-1</sup>, with the solution flowing at  $\sim$ 2 mL min<sup>-1</sup>. All solutions were deaerated by purging with N<sub>2</sub> (Airgas) prior to and during experiments.

Electron probe microanalysis (EPMA) was performed on a JEOL JXA-8600 Superprobe, using 10 µm electron beam diameter, 10 keV accelerating voltage, and 15 nA beam current. Scanning electron microscopy (SEM) and energy-dispersive X-ray spectroscopy (EDS) were performed on a FEI Inspect F50 FEG SEM (FEI, Hillsboro, OR). STM images were obtained in air using a Nanoscope III (Digital Instruments, Santa Barbara, CA) with a tungsten tip. Raman spectra were obtained using a Renishaw inVia Raman microprobe (Renishaw, Wotton-under-edge, U.K.) equipped with a CCD detector. A 514 nm Ar-ion laser (Modu-Laser, LLC, Centerville, UT) running

at 0.67 mW was used as the excitation source. An 1800 lines/mm grating and a 20X objective were used during the spectral acquisition. X-ray photoelectron spectroscopy (XPS) was performed using a Mg K $\alpha_{1,2}$  (STAIB) X-ray source, at  $\sim$ 70° to the hemispherical analyzer axis (Leybold Heraeus). The Au  $4f_{7/2}$  peak at 84.0 eV originating from the substrate was used to calibrate binding energies. Shirley background corrections were applied for each spectrum [33].

Photoelectrochemical (PEC) measurements were performed using light from a 300 W Xe arc lamp (Oriel Instruments, Stratford, CT), dispersed with an Oriel Cornerstone 260 Model 74100 monochromator, equipped with a 1200 lines/mm grating. The light was then chopped at 20 Hz and illuminated onto the MoSe<sub>2</sub> sample through a quartz window. The sample was immersed in 0.1 M NaClO<sub>4</sub>, pH 1.5. The photovoltage was measured as the 20-Hz component of the open-circuit potential, through a lock-in amplifier (Standard Research Systems Model SR830, Sunnyvale, CA).

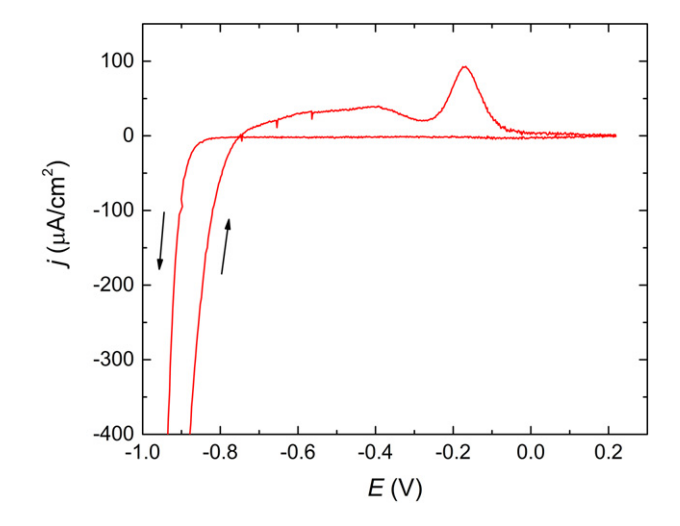
Sample annealing was performed in a tube furnace (Lindberg/Blue Model TF55030A-1, Asheville, NC) in 1%/99% H<sub>2</sub>/Ar (Airgas). The temperature was ramped from room temperature up to the annealing temperature at 5 °C min<sup>-1</sup>. After half an hour at the annealing temperature, it was ramped down to room temperature at no more than 5 °C min<sup>-1</sup>.

#### 3. Results and discussion

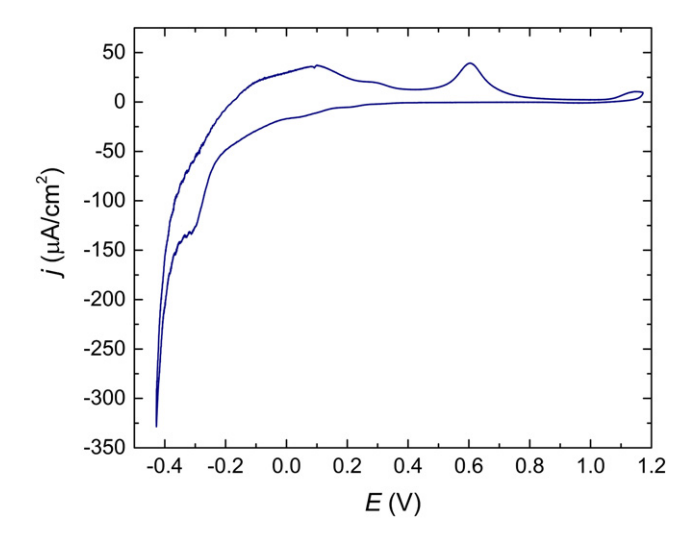
#### 3.1. Voltammetric behavior of Mo and Se

Fig. 1 is a cyclic voltammogram (CV) for Au in 1 mm  $MoO_3$  and 1 m  $NH_4Cl$  (pH 8.3). The scan started negative from 0.06 V, the open-circuit potential (OCP), to -1 V. Reduction began abruptly near -0.85 V. The rapid increase in current at -0.85 V is consistent with the overpotential for the HER on Au. However, on the positive-going scan, the HER ceased near -0.75 V, which is more consistent with the overpotential for the HER on Mo [26]. Positive of -0.75 V, oxidative current was evident in two regions: a broad oxidation feature between -0.75 V and -0.27 V, followed by a Gaussian-shaped peak, at -0.18 V.

The CV of Au in an acidic  $\mathrm{HMoO_4}^-$  solution, pH 1.5, is displayed in Fig. 2. In the negative-going scan from the OCP, 0.42 V, a reductive shoulder was observed at -0.3 V, prior to the onset of HER. This current was attributed to reduction of  $\mathrm{Mo^{VI}}$  species, probably  $\mathrm{HMoO_4}^-$ . At -0.4 V, current for the HER increased rapidly, though no hysteresis was observed in the subsequent positive-going scan, in contrast



**Fig. 1.** CV of Au in a solution of 1 mm MoO<sub>3</sub>, 1 m NH<sub>4</sub>Cl, and 0.1 m NaClO<sub>4</sub> (pH 8.3). Open-circuit potential was 0.06 V. The initial sweep direction was negative from OCP, and the sweep was reversed at -1 V. A hysteresis loop was observed in the HER region, followed by two oxidative features.



**Fig. 2.** CV of Au in 1 mm HMoO $_4$  and 0.1 m NaClO $_4$  (pH 1.5). No NH $_4$ Cl was added to the solution. The open-circuit potential was 0.42 V. The initial sweep was from OCP to -0.43 V. The oxidation features in the reversed sweep are similar to those observed in the pH 8.3 solution.

to Fig. 1 for the pH 8.3 solution. The oxidation features, however, were similar to those in Fig. 1: a broad oxidation, followed by a Gaussian-shaped peak.

For the sake of discussion, it is presumed that elemental Mo is deposited at low potentials; however, it is difficult to prove, under the characterization conditions, that some limited amount of a  $MoO_x$  species was not also present during deposition. Using the flow cell, Mo was deposited onto an Au electrode at -0.41 V for 30 s in the acidic  $HMoO_4^-$  solution. The solution was then replaced with blank at OCP (-0.18 V), and a CV was run with the solution flowing (Fig. 3). The CV started from OCP and scanned in the positive direction to 0.20 V. The broad oxidation was reminiscent of a passivation process [7,34]. After oxidation to 0.20 V, the potential sweep was reversed and scanned to -1.3 V, followed again by an oxidative sweep to 0.2 V

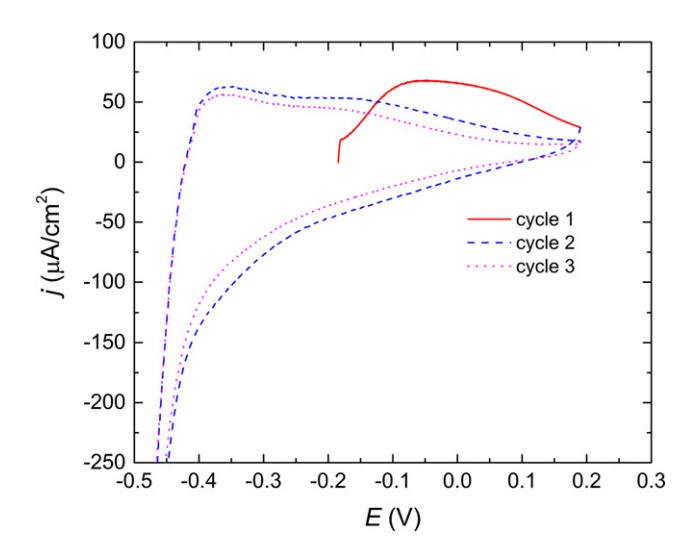


**Fig. 3.** CV of  $MoO_x/Au$  in 0.1 M NaClO<sub>4</sub> blank (pH 1.5). The  $MoO_x$  was deposited at -0.41 V for 30 s in the acidic  $HMoO_4^-$  solution. The open-circuit potential in blank was -0.18 V. In cycles 2 and 3, the negative-going sweep was reversed at -1.3 V. The subsequent broad oxidation feature would disappear if the potential were scanned to 1 V instead of 0.2 V. Cathodic current in the region negative of -0.5 V is not shown because that current was almost entirely associated with HER, with no distinguishable feature for  $MoO_x$  reduction.

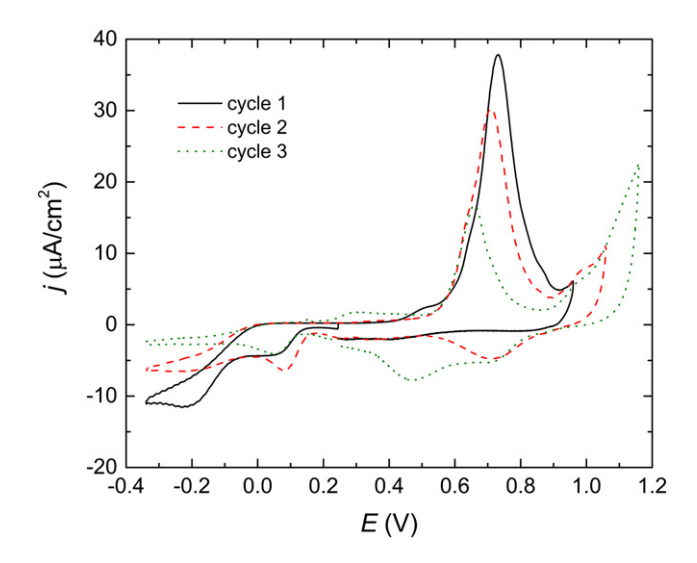


**Fig. 4.** CV of Au in 0.1~mm SeO $_2$  and 0.1~m NaClO $_4$  (pH 5). The open-circuit potential was 0.24~V, and the initial sweep was in the negative direction from the OCP. After scanning to -0.34~V, the subsequent oxidation (onset at 0.5~V) corresponded to no more than 0.5~monolayer of Se on Au.

(Fig. 3, cycle 2) in the blank. The reappearance of the broad oxidation feature in blank indicates that the product of the oxidation was insoluble, and remained on the surface, to be reduced again. On the other hand, by scanning to 1 V (not shown), the insoluble product of the oxidation was further oxidized and became soluble, and on the subsequent cycle the oxidation features, in Fig. 2, disappeared. The Pourbaix diagram suggests that reduction in an acidic  $HMoO_4^-$  solution would result in Mo deposition, and that oxidizing to 0.2 V should form solid  $MoO_2$ , which is consistent with the results above [35]. Scanning to 1 V resulted in conversion of the insoluble  $MoO_2$  to soluble  $HMoO_4^-$ , which was rinsed away by the blank. This dissolution coincides with the "Gaussian" oxidation feature at 0.6 V (Fig. 2). An in situ chemical or spectroscopic probe would be needed to establish the exact number and identities of the oxidized Mo species.

Selenium deposition was also examined as a function of pH. In pH 8.3, no Se deposition was evident in a CV of an Au electrode in 0.1 mm SeO<sub>2</sub>. At pH 5 (Fig. 4), Se deposition appeared to be limited to UPD. The onset of UPD oxidation (cycle 1) was 0.5 V, and resulted in an oxidation charge for Se stripping of around 0.5 monolayer (ML). A ML is defined in this report as one adsorbate (Se) for every substrate surface atom (Au). In pH 1.5, the Se deposition and stripping features (Fig. 5) shift positively. On the negative-going scan, from the OCP (0.43 V), the first two reduction peaks correspond to surface-limited deposition features, similar to UPD, except that they occurred at overpotentials, rather than underpotentials, suggesting slow kinetics [36]. Their corresponding oxidation feature occurred at 0.78 V. The third reduction feature, negative of 0.2 V and down to -0.25 V, corresponds to bulk Se deposition, which oxidized on the positive-going scan in the sharp feature just positive of 0.6 V. The more positive stripping potential (0.78 V) of the Se UPD, the atomic layer of Se in contact with the Au, showed the increased stability, relative to bulk Se (0.6 V), expected for a surface-limited (UPD) process. Negative of −0.25 V, bulk Se was reductively stripped, forming soluble H<sub>2</sub>Se in the peak just positive of -0.4 V. The HER on the Se-coated surface began negative of -0.55 V. Compared to the CV for Au in the HMoO<sub>4</sub> $^$ solution (Fig. 2), the HER overpotential on the Se-terminated surface appeared about 0.2 V larger than on the  $MoO_x$ -coated surface. Given that Mo electrodeposition appeared hindered by extensive hydrogen evolution, suppressing the HER by coating with Se was felt by the authors to be advantageous for inducing Mo deposition and the formation of MoSe<sub>2</sub>.

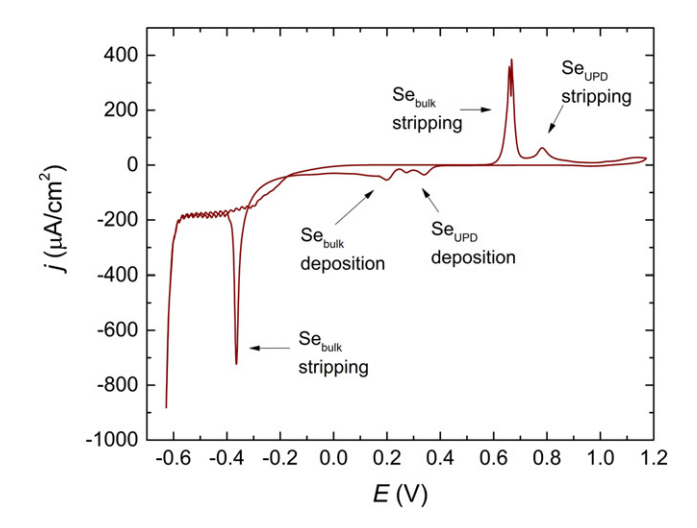


**Fig. 5.** CV of Au in 0.5 mm SeO $_2$  and 0.1 m NaClO $_4$  (pH 1.5). The open-circuit potential was 0.43 V. The potential sweep started in the negative direction from OCP. Se-related reduction and oxidation features are indicated in the CV.

#### 3.2. E-ALD of MoSe<sub>2</sub>

In studies of MoSe<sub>2</sub> deposition, the precursor solutions were 0.5 mm SeO<sub>2</sub> and 1 mm HMoO<sub>4</sub><sup>-</sup>, both adjusted to pH 1.5. A simplified E-ALD cycle scheme for MoSe<sub>2</sub> formation is shown in Fig. 6. Prior to the first MoSe<sub>2</sub> cycle (the dashed region), Se UPD was formed on the Au substrate by flowing the SeO<sub>2</sub> solution at potential E1 (step a). The cycle was then begun by flowing the  ${\rm HMoO_4}^-$  solution at E1 to deposit  $MoO_x$  (step **b**), followed by the  $SeO_2$  solution, again at E1 (step  $\mathbf{c}$ ). The cycle finished with reduction in the SeO<sub>2</sub> solution at a more negative potential, E2, where the MoO<sub>x</sub> was reduced to form  $MoSe_2$  (step **d**). Any excess (bulk) Se should also have reductively stripped at E2. The E-ALD cycle, steps **b** to **d** (Fig. 6), was repeated to grow thicker films. To avoid intermixing the two reactants, a pH 1.5 blank was used between precursor solutions. Current and potential time traces, for one E-ALD cycle, are shown in Fig. 7. The figure also displays solutions and potentials used in each step of the deposition cycle, along with the corresponding current responses.

Oxidative stripping curves were used to characterize preliminary MoSe<sub>2</sub> films, grown using the E-ALD scheme depicted in Fig. 6. The films were formed using E1 = -0.2 V and E2 = -0.4 V. The voltammetry shown in Fig. 8 was for scans from -0.4 V to 1.5 V. For the purposes of comparison, only films formed with 4-, 5- and 6-cycles are shown. A Gaussian-like oxidation peak was observed in each scan, which shifted positively with increasing number of E-ALD cycles, suggesting increasing stability with the number of cycles, or film thickness. It is important to note that the oxidation peaks occurred at potentials more positive than those for  $\text{MoO}_{\chi}$  or bulk Se oxidation (Figs. 2 and 5). It is presumed that the gain in stability results from the presence of  $\text{MoSe}_2$ , a stable compound, as opposed to deposits of the pure elements alone [37,38]. Changes in

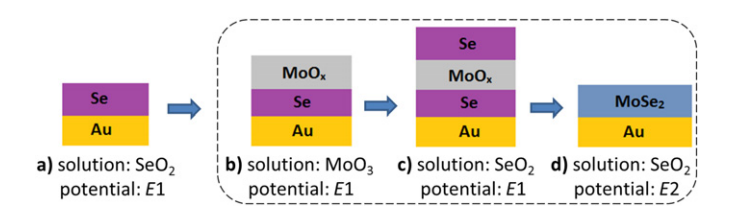


**Fig. 6.** A simplified scheme for forming MoSe<sub>2</sub> by E-ALD. Se UPD on Au is performed at the beginning of a deposition (step **a**). Steps **b** to **d** are iterated to deposit MoSe<sub>2</sub> in an ALD manner. Blank solution rinse steps were used to avoid intermixing HMoO<sub>4</sub><sup>-</sup> and SeO<sub>2</sub> solutions but are excluded in this illustration.

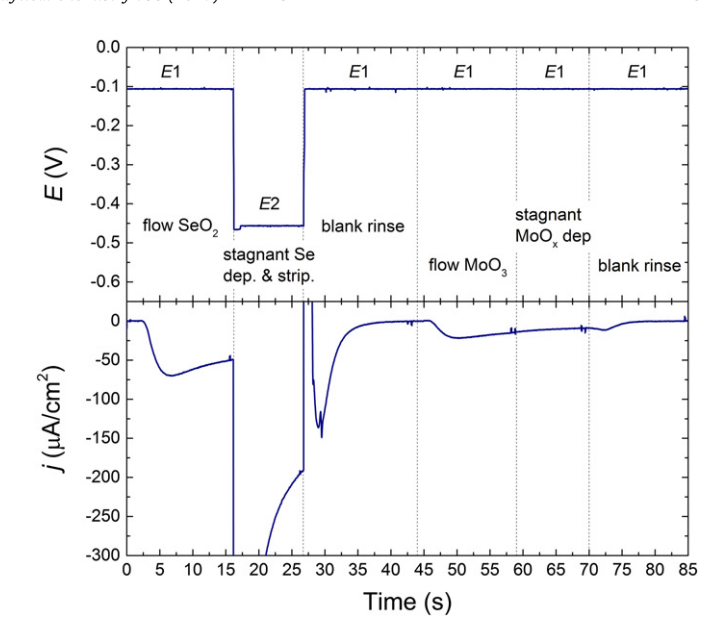


**Fig. 7.** A representative potential profile (top) used in an E-ALD cycle of  $\mathsf{MoSe}_2$ , along with the corresponding current response (bottom) at each step. The vertical dashed lines demarcate the different steps in the cycle. During the solution flow steps, the flow rate was 15 mL min<sup>-1</sup>. No solution flow occurred during the stagnant deposition steps. [SeO<sub>2</sub>] = 0.5 mm. [HMoO<sub>4</sub> $^-$ ] = 1 mm. All solutions (pH 1.5) contained 0.1 m NaClO<sub>4</sub>.

the MoSe<sub>2</sub> films' morphology (larger grain sizes, fewer edge sites, etc.) can also lead to the observed stability gain. The relative amounts deposited in each film were quantified by integration of the charge for oxidative stripping, and they are plotted in the inset of Fig. 8, as a function of the number of E-ALD cycles. The linear increase in coverage with cycle number, expected for an ALD process, demonstrates that thicker films can be deposited by increasing the number of cycles.

Photoelectrochemistry (PEC) was used to characterize a 50-cycle film grown using the same cycle conditions used in Fig. 8. In that study the photovoltage was measured as a function of the photoexcitation energy. The photovoltage was essentially a measurement of changes in the electrode's OCP, arising from photogenerated

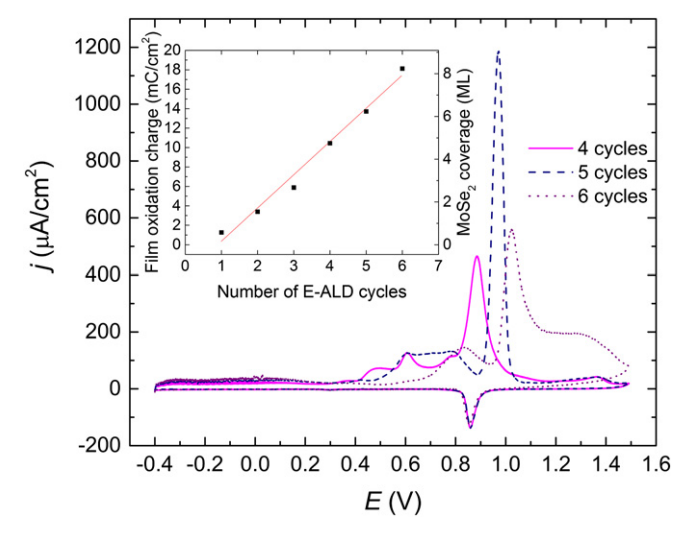


**Fig. 8.** Oxidative stripping voltammograms in blank solution (0.1  $\,\mathrm{M}$  NaClO<sub>4</sub>; pH 1.5) of preliminary MoSe<sub>2</sub> films grown by E-ALD. These films were grown by using  $E1 = -0.2\,\mathrm{V}$  and  $E2 = -0.4\,\mathrm{V}$ . The inset shows the integrated oxidative charge from each film as a function of the number of E-ALD cycles. The MoSe<sub>2</sub> coverage for each cycle was calculated based on a 10-electron oxidation process.

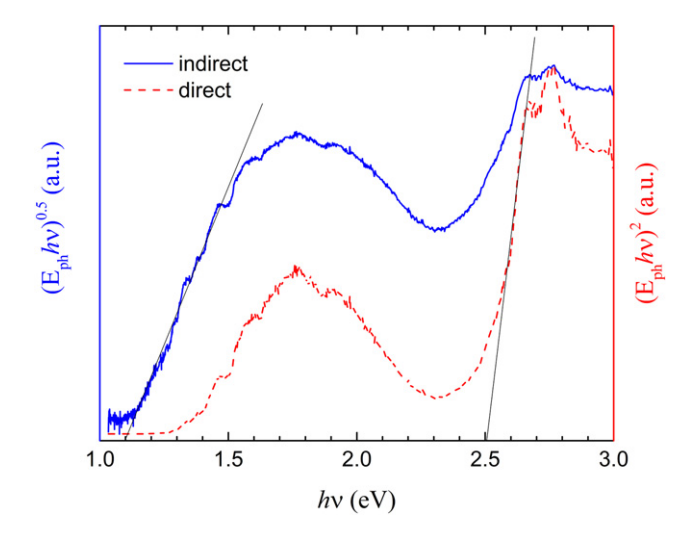


**Fig. 9.** Photovoltage measurement in  $0.1 \text{ m NaClO}_4$  (pH 1.5) of a MoSe<sub>2</sub> film grown by 50 E-ALD cycles. The data was plotted in two different forms that are appropriate for determining either a direct or an indirect band gap. The extrapolated band gap values of 1.1 eV and 2.5 eV correspond to those of MoSe<sub>2</sub> and MoO<sub>2</sub>, respectively.

electron-hole pairs [39]. It was used to indirectly probe the absorption of light by the deposit, since the Au substrate was not transparent. The technique proved convenient for characterizing film optical properties. Fig. 9 shows photovoltage,  $E_{ph}$ , measurements for the 50-cycle film, where  $E_{ph}$  was assumed proportional to the optical absorption coefficient, the premise for plotting data in the form of a Tauc plot for determining an optical bandgap [40]. Two absorption edges suggested the presence of both MoSe<sub>2</sub> and MoO<sub>2</sub> in the film, prompting the construction of two Tauc plots. MoO<sub>2</sub> is known to show a direct transition, while bulk MoSe<sub>2</sub> shows an indirect transition [16,19,41]. Extrapolations of the corresponding absorption edges indicated optical band gaps of 2.5 eV for MoO<sub>2</sub> and 1.1 eV for MoSe<sub>2</sub>, which matched literature values well [42].

To optimize deposition potentials in the cycle, E1 and E2, a first series of 50-cycle deposits were prepared by varying E1 while holding E2 constant at -0.5 V (Fig. 10). A second series was prepared by varying E2 while holding E1 constant at -0.1 V (Fig. 11). Deposit elemental compositions were obtained using EPMA. The Mo content increases as E1 is pushed negatively, as expected from the CV in Fig. 2. On the other hand, the complementary increase in Se content was not expected from the CV in Fig. 5, as the currents at those values

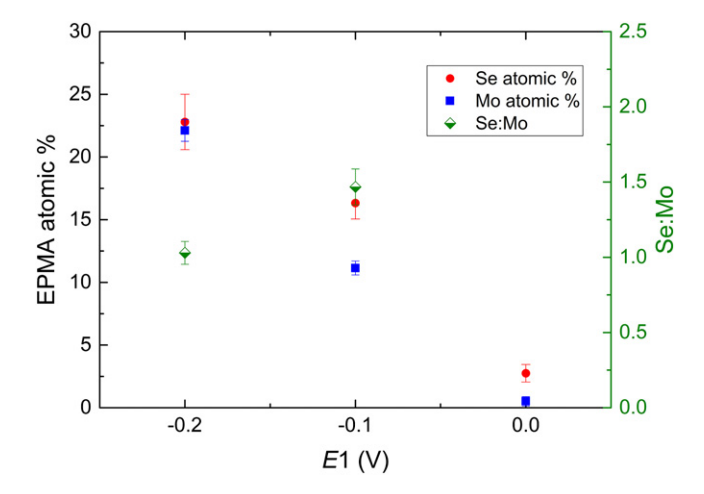


**Fig. 10.** Composition analysis by EPMA for the series of 50-cycle deposits where E1 was varied while holding E2 constant at -0.5 V.

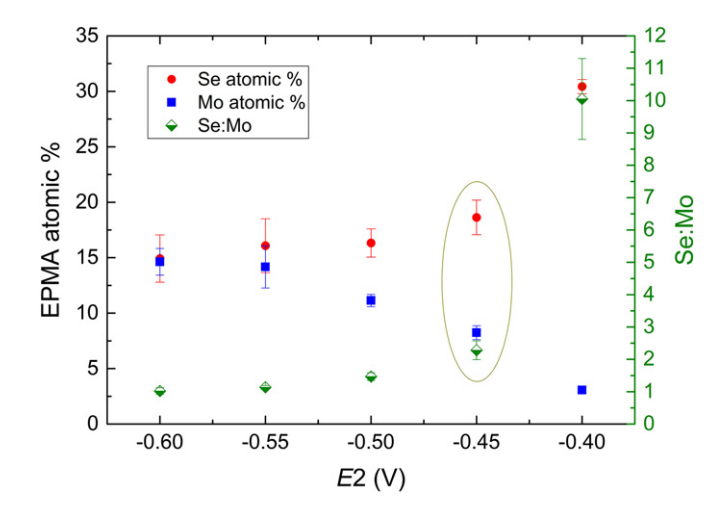


**Fig. 11.** Composition analysis by EPMA for the series of 50-cycle deposits where E2 was varied while holding E1 constant at -0.1 V. The circled composition corresponds to the deposit that had the closest stoichiometric ratio to that of ideal MoSe<sub>2</sub>.

of E1 (from 0 V to -0.2 V) appeared to be the same, i.e., mass-transfer limited. Even if more Se was deposited at the more negative values of E1, during the potential step to E2 (-0.5 V), only Se bound to Mo would be expected to remain on the surface, as any bulk Se (Fig. 5) should have reductively stripped. Those results suggested that as the Mo coverage increased, selenium increased by depositing on the Mo, as would occur in a UPD process.

Fig. 11 shows the composition analysis for the second series of deposits where E1 was held constant at -0.1 V. E2 was varied between -0.4 V and -0.6 V. At -0.4 V, the bulk Se was not removed. However, at E2 = -0.45 V, the stoichiometry for Se:Mo is closest to the expected value of 2. At more negative values of E2, the coverage of Mo increased and then plateaued, while the Se coverage remained essentially constant. If it is presumed that a  $MOO_x$  species is deposited at E1 = -0.1 V, it appears that the kinetics for its reduction with Se to form  $MOSe_2$  are slow and thus potential-dependent. The Mo coverage plateaued at the most negative potentials because the Se coverage was limited during its deposition at E1.  $MOO_x$  species

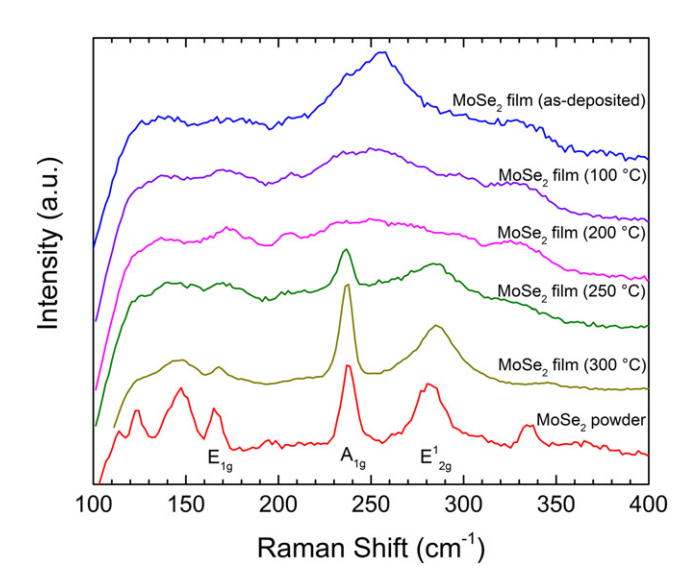


**Fig. 12.** Micro-Raman spectra of some MoSe<sub>2</sub> films annealed at different temperatures. The characteristic  $E_{1g}$ ,  $A_{1g}$ , and  $E_{2g}^1$  peaks of MoSe<sub>2</sub> are apparent after annealing at 250 °C and above. The spectrum of commercial MoSe<sub>2</sub> powder is included for reference.

not reacted with Se became available for oxidation to a soluble species when the potential was stepped back to -0.1 V (E1), while any Mo bonded with Se, as MoSe<sub>2</sub>, was stabilized (Fig. 8). From the series shown in Fig. 11, deposits formed using E2 = -0.45 V and E1 = -0.1 V were selected for annealing studies, based on their Se:Mo ratio.

#### 3.3. Annealing studies

Deposits made using E1 = -0.1 V and E2 = -0.45 V were thermally annealed in a 1%/99%  $\text{H}_2/\text{Ar}$  atmosphere. The Raman spectra as a function of annealing temperature are shown in Fig. 12. A broad asymmetric peak centered at  $256 \text{ cm}^{-1}$  was observed for the asdeposited film. This peak was assigned to a Se-Se stretch mode, arising from a slight Se excess in the film [20]. No other significant changes in the Raman spectra were observed until  $250 \,^{\circ}\text{C}$  or above. At  $250 \,^{\circ}\text{C}$  and above, the well-known  $E_{1g}$ ,  $A_{1g}$  and  $E_{2g}^1$  peaks of MoSe<sub>2</sub> were identified [16,43,44]. Raman spectra from a commercial MoSe<sub>2</sub> powder sample were used for reference.

a

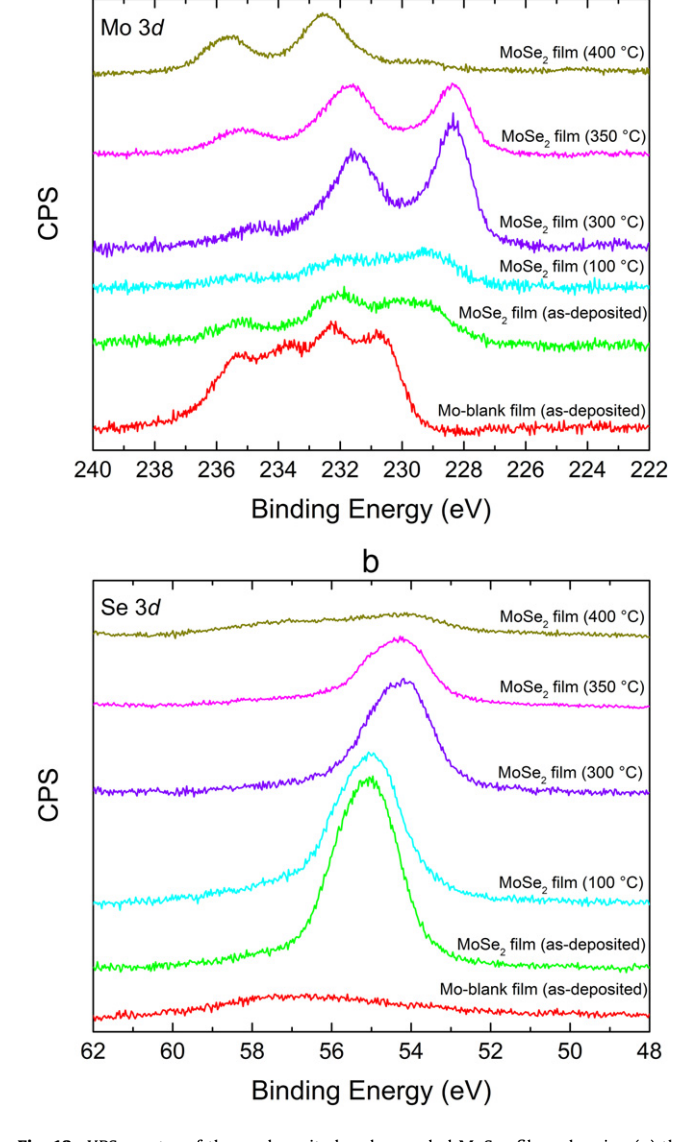


**Fig. 13.** XPS spectra of the as-deposited and annealed MoSe $_2$  films showing (a) the Mo 3d and (b) the Se 3d photoelectric peaks. The "Mo-blank" deposit was formed by using the blank instead of the SeO $_2$  solution within the E-ALD cycles.

XPS was used to follow the effect of annealing on speciation in the surface of the MoSe<sub>2</sub> film. Fig. 13 shows XPS spectra for the Mo 3d and Se 3d regions. The Mo 3d signal from the as-deposited film and the film annealed at 100 °C appeared to originate predominantly from Mo oxides on the surface. At 300 °C and 350 °C, the Mo 3*d* peaks clearly shifted to lower binding energies, more consistent with Mo in MoSe<sub>2</sub> [20,21,45]. Positions of the Mo  $3d_{5/2}$  and Mo  $3d_{3/2}$  doublet were 228.4 eV and 231.7 eV, respectively. The Se 3d peaks also exhibited a similar trend as a function of annealing temperature. At 300 °C and 350 °C, the Se 3d peaks were also shifted to a lower binding energy, consistent with selenide in MoSe<sub>2</sub>. At 400 °C, the film was decomposed to form MoO<sub>3</sub>, presumably due to trace oxygen present in the annealing atmosphere [46,47]. Also shown in Fig. 13 are the XPS spectra of a sample made by replacing the SeO<sub>2</sub> solution with blank during deposition. The resulting deposit consisted entirely of MoO<sub>x</sub>, which displayed Mo 3d peaks with higher binding energies than those of a normal MoSe<sub>2</sub> deposit, indicating that the Se suppressed Mo oxidation by forming MoSe<sub>2</sub>.

Both Raman and XPS data clearly showed the presence of MoSe<sub>2</sub> in samples annealed at 250 °C and above. Although 1% H2 was used during the annealing in an attempt to provide a reducing environment, its effect was deemed negligible. Samples annealed in pure N<sub>2</sub> also showed similar evidence of MoSe<sub>2</sub> by XPS, even though N<sub>2</sub> would not provide a reducing environment, necessary for the formation of  $MoSe_2$  from  $MoO_x$  [19]. Fig. 14 shows the compositions of the annealed deposits from EPMA. As the annealing temperature increased, there was an apparent loss of Se and Mo from the deposits, compared to the as-deposited films. MoSe<sub>2</sub> is thermally stable up to almost 1000 °C, so the loss of Se and Mo content was most likely unreacted Se and MoO<sub>x</sub> in the deposits [48]. Removal of the Se and MoO<sub>x</sub> from the surface by annealing may explain the observed XPS peak shifts. Some MoSe<sub>2</sub> can also be carried off by the gas flux, further contributing to the mass loss. While the annealed samples were amorphous by XRD, their crystallinity could still have been improved by annealing, which would account for the evolution of the MoSe<sub>2</sub> Raman peaks as a function of temperature.

A MoSe<sub>2</sub> sample annealed at 350 °C was imaged by STM and SEM. These images are shown in Fig. 15. The disparity in the shapes of the crystallites between the two images suggests that the circular shapes observed in STM were due to a tip effect. Despite the misleading shapes, the height contrast in the STM image does reveal the stacking nature of the flakes in the sample, consistent with the van der Waals character of the 2D material. Fig. 16 shows an SEM image of the STM tip after it was used to image the MoSe<sub>2</sub> sample. Thin MoSe<sub>2</sub>

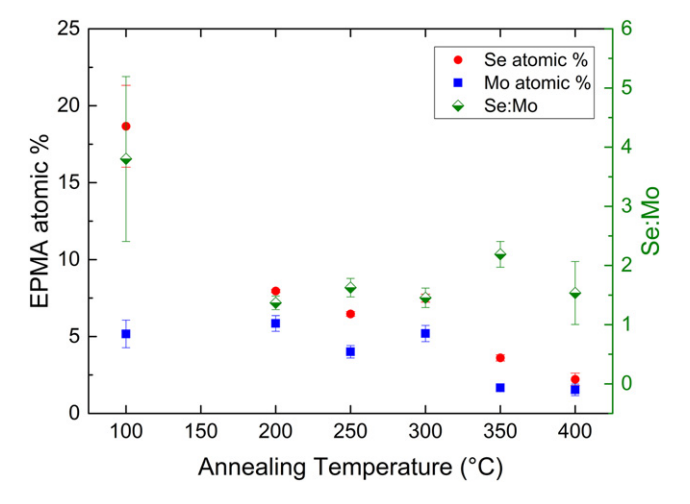


**Fig. 14.** Composition analysis by EPMA of the films annealed at different temperatures. These films were grown using  $E1=-0.1\,\mathrm{V}$  and  $E2=-0.45\,\mathrm{V}$ . Se and Mo losses from the deposits were apparent above 100 °C and 300 °C, respectively.

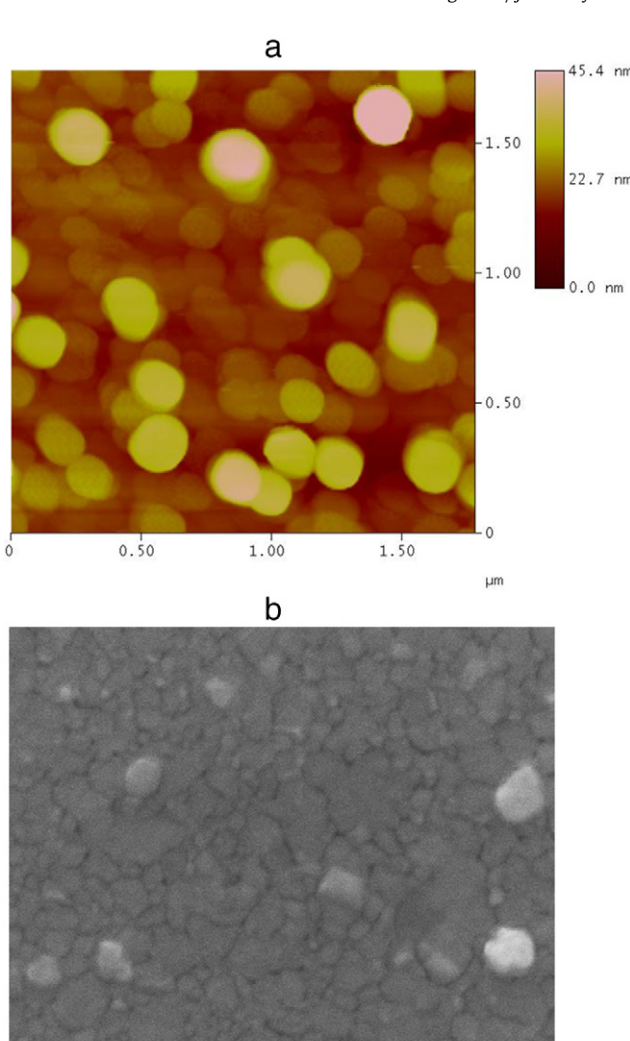


**Fig. 15.** (a) STM and (b) SEM images of a MoSe $_2$  sample annealed at 350 °C. The STM image was acquired in air using a tip-sample bias of -300 mV and a tunneling current of 1 nA.

flakes, confirmed by EDS, appear to have become attached to the W tip during STM imaging, presumably owing to their weak adhesion to the substrate. Some of the flakes on the tip resembled the typical rhombic shapes of MoSe<sub>2</sub> and MoS<sub>2</sub> grown by "chemical vapor deposition" (CVD) [19,49-51].

# 4. Conclusions

The voltammetric behaviors of Au in MoO<sub>3</sub> and SeO<sub>2</sub> solutions were examined under both basic and acidic conditions. Thin films of MoSe<sub>2</sub> were successfully prepared using E-ALD from acidic precursor solutions. PEC photovoltage measurement on the as-deposited films confirmed the presence of MoSe<sub>2</sub> and traces of unreacted MoO<sub>2</sub>. Thermal annealing removed the MoO<sub>2</sub>, enriching the films in MoSe<sub>2</sub>, as confirmed using XPS. The evolution of MoSe<sub>2</sub> Raman peaks as a function of temperature showed that the crystallinity of the films were improved by annealing, though they still appeared amorphous by XRD. Although the film growth conditions have not been fully optimized, this report demonstrated that E-ALD can be used to grow MoSe<sub>2</sub> films. Use of Se to induce the deposition of Mo in order to

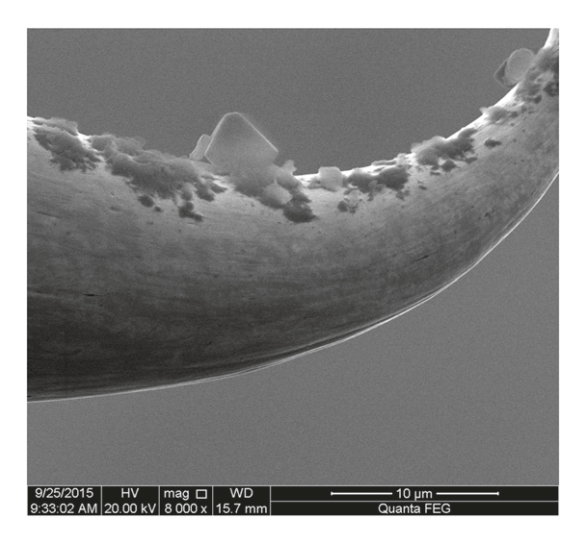


**Fig. 16.** SEM of the STM tip after it was used to image the MoSe<sub>2</sub> sample in air. MoSe<sub>2</sub> flakes, confirmed by EDS, were adhered onto the interior of the tip's curvature.

electrochemically grow MoSe<sub>2</sub> might be applicable to the growth of other transition metal dichalcogenides (TMDC).

#### Acknowledgments

Support for this work, from NSF ECCS, award number 1124733, is gratefully acknowledged. Helpful discussions from Chris Fleisher and for the use of the UGA Electron Microprobe Lab are appreciated. Dr. Zhengwei Pan is also appreciated for the use of his SEM.

#### References

- K.S. Novoselov, A.K. Geim, S.V. Morozov, D. Jiang, Y. Zhang, S.V. Dubonos, I.V. Grigorieva, A.A. Firsov, Electric field effect in atomically thin carbon films, Science 306 (5696) (2004) 666–669.
- [2] Q.H. Wang, K. Kalantar-Zadeh, A. Kis, J.N. Coleman, M.S. Strano, Electronics and optoelectronics of two-dimensional transition metal dichalcogenides, Nat Nano 7 (11) (2012) 699–712.
- [3] M. Chhowalla, H.S. Shin, G. Eda, L.J. Li, K.P. Loh, H. Zhang, The chemistry of two-dimensional layered transition metal dichalcogenide nanosheets, Nature Chemistry 5 (4) (2013) 263–275.
- [4] W.L. McMillan, Landau theory of charge-density waves in transition-metal dichalcogenides, Physical Review B 12 (4) (1975) 1187–1196.
- [5] J. Renteria, R. Samnakay, C. Jiang, T.R. Pope, P. Goli, Z. Yan, D. Wickramaratne, T.T. Salguero, A.G. Khitun, R.K. Lake, A.A. Balandin, All-metallic electrically gated 2H-TaSe<sub>2</sub> thin-film switches and logic circuits, Journal of Applied Physics 115 (3) (2014) 034305.
- [6] Z. Yan, C. Jiang, T.R. Pope, C.F. Tsang, J.L. Stickney, P. Goli, J. Renteria, T.T. Salguero, A.A. Balandin, Phonon and thermal properties of exfoliated TaSe<sub>2</sub> thin films, Journal of Applied Physics 114 (20) (2013) 204301.
- [7] C. Tsang, Y.G. Kim, D. Gebregziabiher, J. Stickney, Ta surface chemistry in aqueous solutions and the possible formation of TaTe<sub>2</sub> and TaS<sub>3</sub>, Journal of the Electrochemical Society 160 (12) (2013) D3278–D3284.
- [8] R.R. Adzic, Electrocatalytic properties of the surfaces modified by foreign metal adatoms, Advances in Electrochemistry and Electrochemical Engineering 13 (1984) 159–260.
- [9] B.W. Gregory, M.L. Norton, J.L. Stickney, Thin-layer electrochemical studies of the underpotential deposition of cadmium and tellurium on polycrystalline Au, Pt and Cu electrodes, Journal of Electroanalytical Chemistry 293 (1-2) (1990) 85–101.
- [10] B.W. Gregory, J.L. Stickney, Electrochemical Atomic Layer Epitaxy (ECALE), Journal of Electroanalytical Chemistry 300 (1-2) (1991) 543–561.
- [11] D.M. Kolb, Physical and electrochemical properties of metal monolayers on metallic substrates, Adv. Electrochem. Electrochem. Eng. 11 (1978) 125–271.
- [12] T.E. Lister, J.L. Stickney, Formation of the first monolayer of CdSe on Au(111) by electrochemical ALE, Applied Surface Science 107 (1996) 153–160.
- [13] V. Venkatasamy, N. Jayaraju, S.M. Cox, C. Thambidurai, U. Happek, J.L. Stickney, Optimization of CdTe nanofilm formation by electrochemical atomic layer epitaxy (EC-ALE), Journal of Applied Electrochemistry 36 (11) (2006) 1223–1229.
- [14] V. Venkatasamy, N. Jayaraju, S.M. Cox, C. Thambidurai, M. Mathe, J.L. Stickney, Deposition of HgTe by electrochemical atomic layer epitaxy (EC-ALE), Journal of Electroanalytical Chemistry 589 (2) (2006) 195–202.

- [15] K.F. Mak, C. Lee, J. Hone, J. Shan, T.F. Heinz, Atomically thin MoS<sub>2</sub>: a new direct-gap semiconductor, Phys. Rev. Lett. 105 (13) (2010) 136805.
- [16] S. Tongay, J. Zhou, C. Ataca, K. Lo, T.S. Matthews, J.B. Li, J.C. Grossman, J.Q. Wu, Thermally driven crossover from indirect toward direct bandgap in 2D semiconductors: MoSe<sub>2</sub> versus MoS<sub>2</sub>, Nano Letters 12 (11) (2012) 5576–5580.
- [17] Y. Zhang, T.R. Chang, B. Zhou, Y.T. Cui, H. Yan, Z.K. Liu, F. Schmitt, J. Lee, R. Moore, Y.L. Chen, H. Lin, H.T. Jeng, S.K. Mo, Z. Hussain, A. Bansil, Z.X. Shen, Direct observation of the transition from indirect to direct bandgap in atomically thin epitaxial MoSe<sub>2</sub>, Nature Nanotechnology 9 (2) (2014) 111–115.
- [18] O. Lopez-Sanchez, D. Lembke, M. Kayci, A. Radenovic, A. Kis, Ultrasensitive photodetectors based on monolayer MoS<sub>2</sub>, Nature Nanotechnology 8 (7) (2013) 497–501.
- [19] X.L. Wang, Y.J. Gong, G. Shi, W.L. Chow, K. Keyshar, G.L. Ye, R. Vajtai, J. Lou, Z. Liu, E. Ringe, B.K. Tay, P.M. Ajayan, Chemical vapor deposition growth of crystalline monolayer MoSe<sub>2</sub>, ACS Nano 8 (5) (2014) 5125–5131.
- [20] F.H. Saadi, A.I. Carim, J.M. Velazquez, J.H. Baricuatro, C.C.L. McCrory, M.P. Soriaga, N.S. Lewis, Operando synthesis of macroporous molybdenum diselenide films for electrocatalysis of the hydrogen-evolution reaction, ACS Catalysis 4 (9) (2014) 2866–2873.
- [21] H.T. Wang, D.S. Kong, P. Johanes, J.J. Cha, G.Y. Zheng, K. Yan, N.A. Liu, Y. Cui, MoSe<sub>2</sub> and WSe<sub>2</sub> nanofilms with vertically aligned molecular layers on curved and rough surfaces, Nano Letters 13 (7) (2013) 3426–3433.
- [22] H. Tributsch, Hole reactions from d-energy bands of layer type group VI transition metal dichalcogenides: new perspectives for electrochemical solar energy conversion, Journal of the Electrochemical Society 125 (7) (1978) 1086–1093.
- [23] A.J. Bard, R. Parsons, J. Jordan, Standard Potentials in Aqueous Solution, Marcel Dekker, Inc., New York, 1985.
- [24] P. Enghag, Encyclopedia of the Elements, Wiley-VCH Verlag GmbH & Co. KGaA. 2007, 589–604. chap. 25
- [25] T.J. Morley, L. Penner, P. Schaffer, T.J. Ruth, F. Benard, E. Asselin, The deposition of smooth metallic molybdenum from aqueous electrolytes containing molybdate ions, Electrochemistry Communications 15 (1) (2012) 78–80.
- [26] R. Syed, S.K. Ghosh, P.U. Sastry, G. Sharma, R. Hubli, J.K. Chakravartty, Electrodeposition of thick metallic amorphous molybdenum coating from aqueous electrolyte, Surface & Coatings Technology 261 (2015) 15–20.
- [27] N.R. Elezovic, V.D. Jovic, N.V. Krstajic, Kinetics of the hydrogen evolution reaction on Fe-Mo film deposited on mild steel support in alkaline solution, Electrochimica Acta 50 (28) (2005) 5594–5601.
- [28] E. Pellicer, E. Gomez, E. Valles, Use of the reverse pulse plating method to improve the properties of cobalt-molybdenum electrodeposits, Surface & Coatings Technology 201 (6) (2006) 2351–2357.
- [29] T.J.S. Anand, C. Sanjeeviraja, M. Jayachandran, Preparation of layered semiconductor (MoSe<sub>2</sub>) by electrosynthesis, Vacuum 60 (4) (2001) 431–435.
- [30] S. Chandra, S.N. Sahu, Electrodeposited semiconducting molybdenum selenide films. I. Preparatory technique and structural characterisation, Journal of Physics D: Applied Physics 17 (10) (1984) 2115.
- [31] S.M. Delphine, M. Jayachandran, C. Sanjeeviraja, Pulsed electrodeposition and characterization of molybdenum diselenide thin film, Materials Research Bulletin 40 (1) (2005) 135–147.
- [32] P.P. Hankare, P.A. Chate, S.D. Delekar, V.M. Bhuse, M.R. Asabe, B.V. Jadhav, K.M. Garadkar, Structural and opto-electrical properties of molybdenum diselenide thin films deposited by chemical bath method, Journal of Crystal Growth 291 (1) (2006) 40–44.

- [33] D.A. Shirley, High-resolution X-ray photoemission spectrum of valence bands of gold, Physical Review B 5 (12) (1972) 4709.
- [34] S.B. Emery, J.L. Hubbley, D. Roy, Voltammetric and amperometric analyses of electrochemical nucleation: electrodeposition of copper on nickel and tantalum, Journal of Electroanalytical Chemistry 568 (1-2) (2004) 121–133.
- [35] M. Pourbaix, Atlas of Electrochemical Equilibria in Aqueous Solutions, Pergamon Press. 1966.
- [36] B.M. Huang, T.E. Lister, J.L. Stickney, Se adlattices formed on Au(100), studies by LEED, AES, STM and electrochemistry, Surface Science 392 (1-3) (1997) 27–43.
- [37] T.A. Sorenson, B.K. Wilmer, J.L. Stickney, Electrochemical digital etching: atomic level studies of CdTe(100), Solid-Liquid Electrochemical Interfaces 656 (1997) 115–125.
- [38] J.L. Stickney, S.D. Rosasco, B.C. Schardt, T. Solomun, A.T. Hubbard, B.A. Parkinson, Demonstration of the surface stability of the van der Waals surface (0001) of MoSe<sub>2</sub> by LEED and electrochemistry, Surface Science 136 (1) (1984) 15–22.
- [39] N. Sato, Electrochemistry at Metal and Semiconductor Electrodes, Elsevier, Amsterdam, New York, 1998.
- [40] O. Stenzel, The Physics of Thin Film Optical Spectra: An Introduction, Springer Series in Surface Sciences, Springer, Berlin, 2005.
- [41] N. Dukstiene, D. Sinkeviciute, Photoelectrochemical properties of MoO<sub>2</sub> thin films, Journal of Solid State Electrochemistry 17 (4) (2013) 1175–1184.
- [42] K.K. Kam, B.A. Parkinson, Detailed photocurrent spectroscopy of the semiconducting Group-VI transition-metal dichalcogenides, Journal of Physical Chemistry 86 (4) (1982) 463–467.
- [43] S. Larentis, B. Fallahazad, E. Tutuc, Field-effect transistors and intrinsic mobility in ultra-thin MoSe<sub>2</sub> layers, Applied Physics Letters 101 (22) (2012) 223104.
- [44] H. Terrones, E.D. Corro, S. Feng, J.M. Poumirol, D. Rhodes, D. Smirnov, N.R. Pradhan, Z. Lin, M.A.T. Nguyen, A.L. Elas, T.E. Mallouk, L. Balicas, M.A. Pimenta, M. Terrones, New first order Raman-active modes in few layered transition metal dichalcogenides, Scientific Reports 4 (2014) 4215.
- [45] W.A. Abdallah, A.E. Nelson, Characterization of MoSe<sub>2</sub>(0001) and ion-sputtered MoSe<sub>2</sub> by XPS, Journal of Materials Science 40 (9-10) (2005) 2679–2681.
- [46] P.M. Magie, A review of properties and potentials of new heavy metal derivative solid lubricants, Lubrication Engineering 22 (7) (1966) 262.
- [47] H.Q. Shi, X.D. Zhou, Y.S. Lin, X. Fu, Synthesis of MoSe<sub>2</sub> nano-flakes modified with dithiophosphinic acid extractant at low temperature, Materials Letters 62 (21-22) (2008) 3649–3651.
- [48] W.A. Brainard, Thermal Stability and Friction of the Disulfides, Diselenides, and Ditellurides of Molybdenum and Tungsten in Vacuum (10<sup>-9</sup> to 10<sup>-6</sup> torr), Tech. Rep. Nasa-TN-D-5141, Lewis Research Center. 1969,
- [49] Y.H. Chang, W. Zhang, Y. Zhu, Y. Han, J. Pu, J.K. Chang, W.T. Hsu, J.K. Huang, C.L. Hsu, M.H. Chiu, T. Takenobu, H. Li, C.I. Wu, W.H. Chang, A.T.S. Wee, L.J. Li, Monolayer MoSe<sub>2</sub> grown by chemical vapor deposition for fast photodetection, ACS Nano 8 (8) (2014) 8582–8590.
- [50] X.D. Duan, C. Wang, J.C. Shaw, R. Cheng, Y. Chen, H.L. Li, X.P. Wu, Y. Tang, Q.L. Zhang, A.L. Pan, J.H. Jiang, R.Q. Yu, Y. Huang, X.F. Duan, Lateral epitaxial growth of two-dimensional layered semiconductor heterojunctions, Nature Nanotechnology 9 (12) (2014) 1024–1030.
- [51] X. Ling, Y.H. Lee, Y.X. Lin, W.J. Fang, L.L. Yu, M.S. Dresselhaus, J. Kong, Role of the seeding promoter in MoS<sub>2</sub> growth by chemical vapor deposition, Nano Letters 14 (2) (2014) 464–472.